Enhanced thermal stability of Ni/GeSn system using pre-amorphization by implantation

A. Quintero, F. Mazen, P. Gergaud, N. Bernier, J.-M. Hartmann, V. Reboud, Eric Cassan, Ph. Rodriguez

Enhanced thermal stability of Ni/GeSn system using pre-amorphization by implantation

A. Quintero,[1,2] F. Mazen,[1] P. Gergaud,[1] N. Bernier,[1] J.-M. Hartmann,[1] V. Reboud,[1] E. Cassan,[2] and Ph. Rodriguez[1,a)]

AFFILIATIONS

[1]Université Grenoble Alpes, CEA, Leti, F-38000 Grenoble, France
[2]Université Paris-Saclay, CNRS, Centre de Nanosciences et de Nanotechnologies, 91120 Palaiseau, France

[a)]**Author to whom correspondence should be addressed:** philippe.rodriguez@cea.fr

ABSTRACT

Improving the thermal stability of Ni/GeSn intermetallics is of great importance to avoid surface degradation and Sn segregation. For this purpose, we studied the effects of pre-amorphization by ion implantation (PAI) of GeSn layers prior to metallization. The impact of Si, Ge, C, or Ge + C PAI was evaluated in terms of phase sequence, morpohological, and electrical evolution during the solid-state reaction. The overall phase sequence, followed by *in situ* x-ray diffraction, was comparable with or without PAI and went as follows: the $Ni_5(GeSn)_3$ hexagonal phase was obtained first, followed by the mono-stanogermanide phase: Ni(GeSn). Nevertheless, the threshold temperature for phase formation varied. These variations, depending on the nature of the implanted ions, can be related to kinetic and/or thermodynamic factors as supported by the analysis of bibliography for silicides and germanides. Additionally, it was reported that the use of Si or Ge implantation did not significantly impacted the surface morphology of the layers. On the other hand, the implantation of C positively impacts the surface morphology evolution by delaying Sn long-range diffusion and Ni(GeSn) agglomeration. This trend was then highly beneficial for preserving electrical stability in an enhanced process window.

I. INTRODUCTION

The use of GeSn layers is interesting for electronic or opto-electronic applications. For electronic applications, this material can be used (i) as source and drain stressors in Ge Metal Oxide Semiconductor Field-Effect Transistors (MOSFETs) (ii) as the channel material of high mobility p-MOSFETs and (iii) in innovative architectures like fin field-effect transistor (FinFETs) or Tunnel Field-Effect Transistors (TFETs).[1–3] On the other hand, opto-electronic applications can greatly benefit from the indirect–direct bandgap transition that can be achieved with Sn introduction in the Ge lattice.[4]

Nickel (Ni) intermetallics have been proposed in order to contact GeSn-based electronic or opto-electronic devices, thanks to the low temperature required for their formation and the low values of contact R_c and sheet R_{sh} resistances achieved.[5–7] However, the phase stability of Ni-stanogermanides is low: high defect densities together with agglomeration and Sn segregation were evidenced with the increase of the annealing temperatures.[6,8–10] These stability problems can negatively impact the electrical properties of the intermetallics, reducing the quality and reliability of contacts.

Similar problems were observed for Ni-silicides: NiSi resistivity collapses due to the agglomeration and nucleation of a higher resistivity phase ($NiSi_2$). The addition of alloying elements such as Pt or Co was shown to enhance silicides, thermal stability.[11–14] Recently,[15,16] we had demonstrated that the addition of 10 at. % of Pt into the Ni metallization layer stabilized the surface morphology, the electrical properties, and delayed Sn segregation of GeSn-based systems. The addition of 10 at. % of Co can also push toward higher values the Sn segregation temperature for Ni/GeSn intermetallics.[16] Another alternative approach involves modifying the semiconductor layer prior to the metallization step by Pre-Amorphization Implantation (PAI). For silicides, this additional process increased the thermal stability of the Ni-silicide and decreased its interface roughness with silicon.[17] Tsui *et al.*[18] showed that the implantation of high doses of Ge resulted in very smooth NiSi/Si interfaces with higher thermal stability, while the $NiSi_2$ phase formation was delayed. Mao *et al.*[19,20] demonstrated that Ge PAI promoted Ti-silicidation and Ti-germanosilicidation at lower temperatures while improving the electrical properties. On the other hand, Liu *et al.*[21] examined the impact of C

pre-stanogermanidation implant with a dose of 1×10^{15} cm^{-2} and energies of 2 keV in GeSn layers with 4 at. % of Sn in substitutional sites. They showed that the thermal stability could be increased by this method. Additionally, surface degradation was delayed and electrical properties were improved.

Ion implantation is, thus, envisioned as an alternative to improve stability in high Sn at. % content GeSn-based layers in order to benefit from high quality metallic contacts. This study evaluated the effect of the pre-amorphization implantation by Si, Ge, C or Ge + C in GeSn with 10 at.% of Sn content prior to Ni metallization. The impact of these processes in terms of phase sequence and morphological and electrical properties was analyzed during the solid-state reaction.

II. EXPERIMENTAL

GeSn layers having a thickness of 60 nm with 10 at.% of Sn in substitutional sites were epitaxially grown at 325 °C, 1.33×10^4 Pa on Ge-buffered Si (1 0 0) substrates using reduced pressure chemical vapor deposition (RPCVD). Sn content was measured from ω-2θ XRD scans around the (4 0 0) Ge reflection assuming the fact that GeSn layers were fully compressively strained on Ge strain relaxed buffers (SRBs) underneath.[22] PAI was conducted in a conventional 300 mm ion implanter. The following parameters were used: 2.8×10^{14} at/cm^2 of Si at 10 keV, 1×10^{14} at/cm^2 of Ge at 20 keV, 3.5×10^{15} at/cm^2 of C at 5 keV, or a combination of Ge + C. These parameters were adjusted to obtain an amorphous GeSn thickness of 25–30 nm by simulations. The simulations were made with the CTRIM code, which has been properly detailed by Posselt and Biersack.[23] A calibration was made by Koffel for pure Ge.[24] With it, it is possible to calculate the profile of implanted ions, the profile of generated defects, and even the position of the amorphous/crystal limit. We considered for our case that the GeSn layers would have similar properties to pure Ge. Then, a surface preparation with Ar plasma for 60 s was performed followed by the deposition, at room temperature, of 10 nm of a Ni layer capped with 7 nm of TiN by magnetron sputtering. Ar plasma conditions were optimized in a previous study[25] and were chosen to minimize the impact on the surface.

The phase formation sequence and crystalline evolution were monitored by *in situ* x-ray diffraction (XRD) using an Empyrean PANalytical x-ray diffractometer equipped with a copper (Cu Kα) source, a linear detector (PIXcel^{1D}), and an HTK 1200 Anton Paar furnace under secondary vacuum (pressure was maintained at about 0.1 Pa to avoid atmospheric contamination). θ–2θ scans were performed with a 2° offset in ω in order to attenuate the symmetric (4 0 0) substrate reflection. Profiles were acquired from 50 to 700 °C with 5 °C steps and a scanning time of 7 min per temperature step.

In addition, samples were annealed in a rapid thermal annealing (RTA) furnace in a N_2 environment for 30 s at temperatures ranging from 150 to 550 °C. Then, complementary θ–2θ scans using a Cu source were performed using an X'Pert Pro PANalytical x-ray diffractometer. Phase analysis was performed with the HighScore Plus software from PANalytical using the International Centre for Diffraction Data (ICDD) PDF-4 database. For samples annealed by RTA, the evolution of the surface morphology and the electrical properties were quantified by tapping mode atomic force microscopy (AFM) in a Bruker FastScan equipment and sheet resistance (R_{sh}) with a four-point probe meter.

Energy-dispersive x-ray spectrometry (EDS) measurements were performed using a probe-corrected FEI Titan microscope operated at 200 kV. EDS spectra were acquired using the four windowless silicon drift detectors (SDD) integrated into the pole piece, which enabled x-ray detection over a 0.8 srad solid angle. EDS spectra were acquired, thanks to a Gatan Microscopy Suite 3 (GMS3) software with a dwell time of 0.05 s. The pixel size was approximately 1 nm for all maps.

III. RESULTS AND DISCUSSION

A. Impact on phase formation sequence

The phase sequences followed by *in situ* XRD of a reference sample (i.e., without any PAI treatment but processed and analyzed under the same conditions as PAI-treated samples), and a C PAI-treated sample are shown in Fig. 1 as contour maps. The y axis shows the temperature, and the x axis shows the diffraction angles. Whatever be the sample analyzed, from the as-deposited state and at low temperatures, characteristic peaks of TiN (1 1 1) at 36.4°, Ni (1 1 1) at 44.9°, Si (4 0 0) and Ge/GeSn (4 0 0) around 67.0° were observed.

As far as the reference sample is concerned and since the as-deposited state, diffraction peaks at 46.5° and 86.0° are discernible. In agreement with previous results, these peaks were due to the growth of the ε-$Ni_5(GeSn)_3$ rich phase.[10] At around 120 °C, these peaks progressively shifted toward higher 2θ angles, and the Ni layer was totally consumed. This shift was linked to stoichiometry variations, i.e., lattice constant fluctuation of the hexagonal metastable ε-$Ni_5(GeSn)_3$ phase when the Ge(Sn) composition varied.[10]

At 220 °C [marked by a dashed line in Fig. 1(a)], the diffraction peaks linked to the Ni-rich phase dissipated and new diffractions peaks appeared at 42.3°, 44.9°, and 53.6°. They were due to the formation of the Ni-mono-stanogermanide phase Ni(GeSn). This phase remained stable up to 660 °C. At this temperature, the dissipation of the diffraction peaks was related to a phase destabilization when reaching temperatures close to the NiGe–Ge eutectic point.[26]

For the sample treated with C PAI, the phase sequence is, overall, the same. Some discrepancies were, however, observed. In particular, the diffraction peak due to Ni vanished as early as 95 °C and at 105 °C two diffraction peaks linked to the Ni-rich phase appeared at 44.6 ° and 46.5 °. These peaks progressively shifted toward slightly higher 2θ angles above 150 °C. At 270 °C [marked by a dashed line in Fig. 1(b)], the diffraction peaks linked to the Ni-rich phase dissipated and new diffraction peaks appeared at 45.0 ° and 53.4 °. They were due to the formation of the Ni-mono-stanogermanide phase Ni(GeSn). This phase remained stable up to 680 °C.

In order to study the potential impact of the PAI step on phase formation sequences, similar *in situ* XRD analyses were performed on Ni/GeSn systems with Si, Ge, or Ge + C implantation prior to metallization. Figure 2 presents the main differences observed.

The phase sequence is, overall, the same for all the systems. The Ni layer was consumed to the benefit of a Ni-rich phase $Ni_5(GeSn)_3$ which was later consumed to form the Ni-mono-stanogermanide

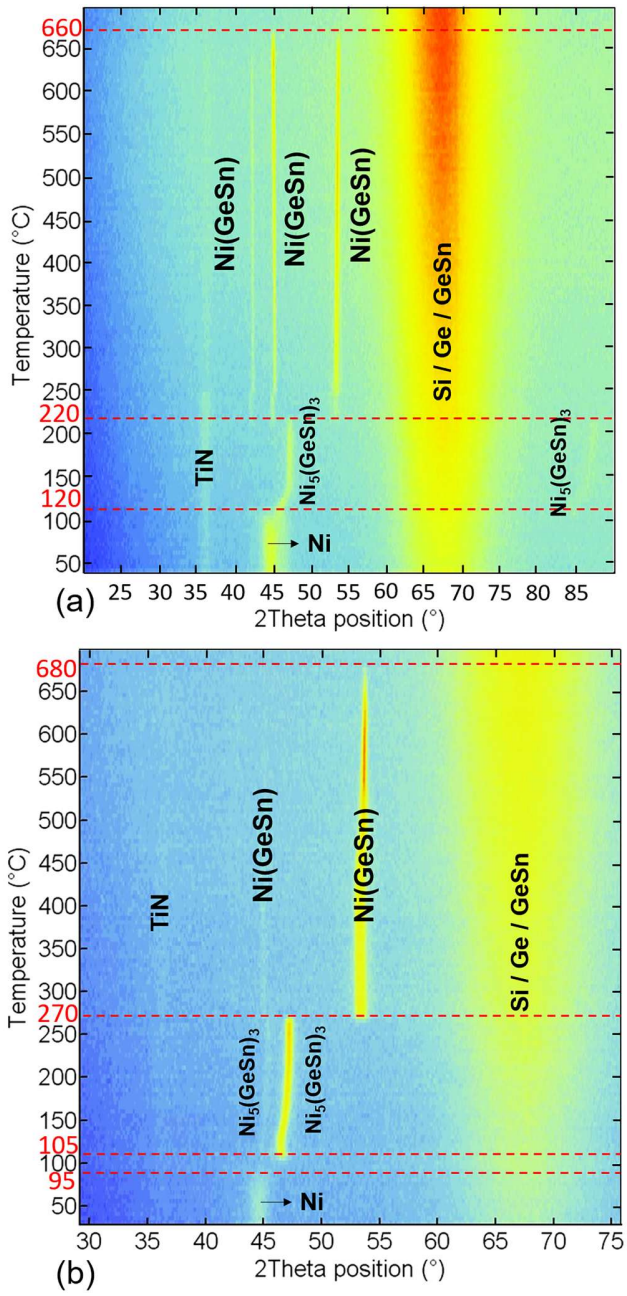

FIG. 1. *In situ* XRD patterns measured during the solid-state reaction of 10 nm of Ni and $Ge_{0.9}Sn_{0.1}$: (a) without PAI and (b) with C PAI.

phase Ni(GeSn). Nevertheless, phase thermal stability differences were observed and are summarized in Table I.

Figure 3 shows the evolution of the Ni (1 1 1) diffraction peak intensity for each system.

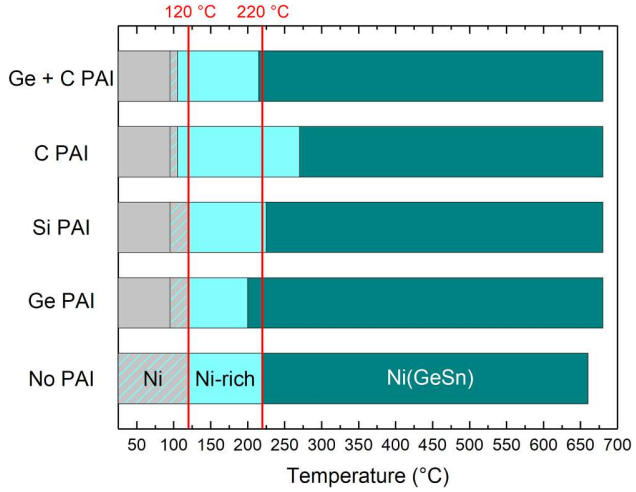

FIG. 2. Summary of the phase formation sequences obtained during the solid-state reaction between 10 nm of Ni and $Ge_{0.9}Sn_{0.1}$ layers without PAI and with various PAI treatments (Ge, Si, C, or Ge + C). Stripped zones show temperature ranges over which the Ni and Ni-rich phases were present simultaneously.

For the reference sample, the Ni consumption was observed at 120 °C, whereas for samples treated by PAI, the Ni XRD peak vanished at 95 °C. It can also be observed that the Ni peak intensity of the reference sample is greater than that of the PAI samples. In addition to the difference between non-implanted sample and implanted samples, one can notice a slight difference between samples implanted with C and samples implanted with Ge or Si. Performing PAI on semiconductor substrates modifies the crystalline structure, with disorder promoting the generation of defects (vacancies and interstitial sites, amorphous region).[27] In addition, the ion mass can affect the amorphization mechanism.[28] Yet, the local properties of the amorphized GeSn layer can vary depending on the ion size, chemical properties, and concentration.

Without any PAI treatment, the as-deposited Ni was highly textured, i.e., the intensity of the diffraction peak observed at 44.9 °C was high. For the PAI-processed samples, the substrate disorder caused by implantation can impact the Ni microstructure,

TABLE I. Threshold temperatures during the Ni/GeSn phase sequence for the reference and PAI-treated samples.

System	Ni consumption	$Ni_5(GeSn)_3$ growth	Ni (GeSn) growth (°C)	Ni(GeSn) destabilization (°C)
Reference	120 °C	As-deposited	220	660
Ge PAI	95 °C	120 °C	200	680
Si PAI	95 °C	120 °C	225	680
C PAI	95 °C	105 °C	270	680
Ge + C PAI	95 °C	105 °C	215	680

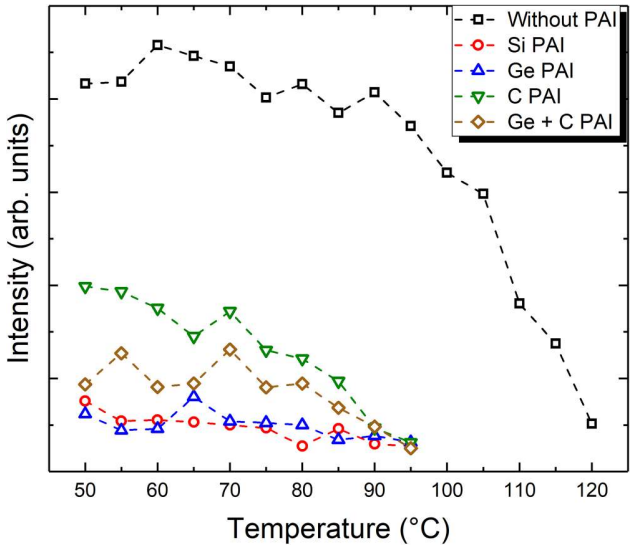

FIG. 3. Comparison of the intensity evolution, with temperature, of the Ni (1 1 1) XRD peak for the reference system and systems with Si, Ge, C, or Ge + C PAI.

i.e., the Ni film was less textured. The peak intensity (that, in a first order, can be linked to a degree of texturation) appeared to be also dependent on the ion mass/size.

Thus, the initial microstructure of Ni is probably governed by the initial state of the GeSn layer. Then, the microstructure of Ni might have an impact on the texture of the Ni-rich phase, which will, in turn, have an influence on the final texture of the monostanogermanide phase. This assertion is supported by the analysis of the out-of-plane orientations of the Ni-rich phase and the monostanogermanide phase (see Fig. 1). The number, the position, and the relative intensities of diffraction peaks related to these phases are different between the reference sample and the samples treated by PAI. A full analysis of this phenomenon is out of the scope of the current study but, with all proportions guarded, it might be linked to the texture inheritance reported for the Ni/Si system.[29–31] Briefly, texture inheritance between one phase and another allows a reaction pathway with a lower activation energy than the expected formation through thermodynamically stable phases.

Finally, as the intensity of the Ni diffraction peak was much weaker for the PAI-treated samples than that for the reference sample (see Fig. 3), the extraction of the intensity values after 95 °C was difficult. Thus, the Ni consumption values reported in Table I for PAI samples could be slightly underestimated.

For the reference system, the Ni-rich phase appeared since the occurrence of the as-deposited state, whereas for all PAI-treated samples, the Ni-rich phase was observed around 105–120 °C. This can be due to solid-state amorphization (SSA) in which, upon annealing, the first interlayer formed is an amorphous phase, even when one or both initial phases are (poly)crystalline.[32] Transmission Electron Microscopy, coupled with Energy-Dispersive Spectroscopy (TEM/EDS) analyses of Ge and Ge + C PAI samples in Fig. 4, revealed indeed the presence of an intermixing layer in which Ni, Ge, and Sn atoms were present even when no other intermetallic phase was identified by XRD.

PAI treatment can promote the formation of a layer by SSA that will later (after going over the 105–120 °C threshold temperature in our case) crystallize to form a Ni-rich layer. The presence of foreign species (Si, Ge, C, or a combination of these species) can impact the nucleation of the first crystalline phases. In addition, the impact of substrate damage caused by the implantation on the Ni-rich phase temperature window was already reported for the Ni/Si system.[33] In our case, the temperature at which the Ni-rich phase disappeared for the samples treated by Ge and Si implantation is almost equivalent to the one observed for the reference sample. On the contrary, the temperature window of the Ni-rich phase is extended when C implantation is used.

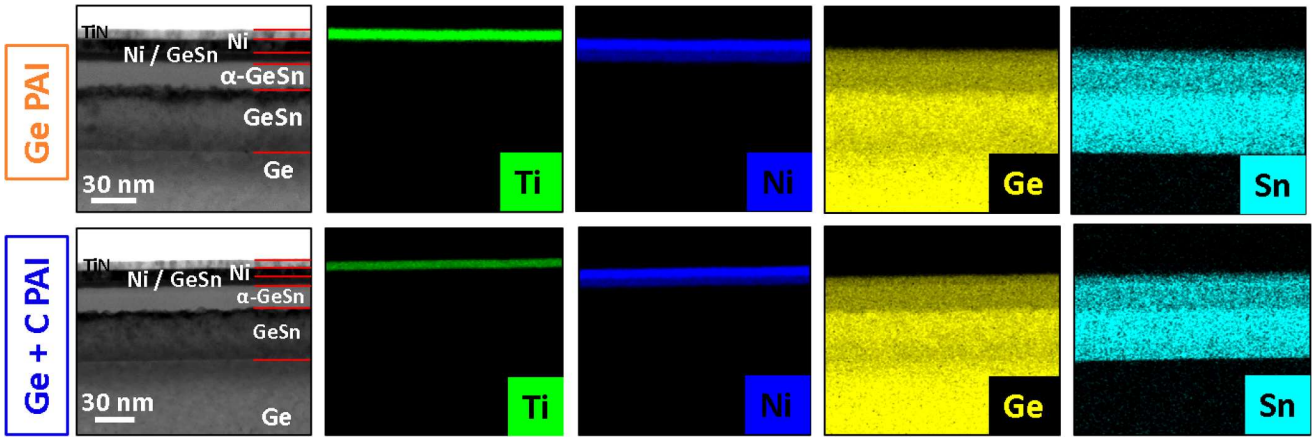

FIG. 4. Cross-sectional TEM images, coupled with an EDS analysis of Ni/GeSn samples with Ge PAI (top row) and Ge + C PAI (bottom row), in the as-deposited state.

Concerning the Ni(GeSn) growth, a variation of the threshold temperature for phase formation (and, thus, Ni-rich phase disappearance) was observed, when the implanted ion varied (see Table I). For the reference sample, the Ni(GeSn) phase appeared after annealing up to 220 °C. Ge PAI decreased the threshold temperature for the Ni(GeSn) growth (200 °C). Meanwhile, Si PAI slightly increased the growth temperature (225 °C). Finally, C PAI postponed the phase growth up to 270 °C. As for the Ni-rich phase, the impact of implantation on the stability of the monophase was observed for the Ni/Si system.[33]

Performing PAI processes promotes the generation of defects (vacancies and interstitial sites, amorphous regions).[27] Mass transport in solids is mediated by these kinds of defects (vacancies, interstitial or complex associations of these defects).[34,35] Then, the increase of defects in the implanted area can influence the reaction kinetics. Changes could be noticed either through a direct impact on the nucleation of the phases or through a modification of the atomic diffusion characteristics, which might modify the phase sequence during the solid-state reaction.[36]

Kittl *et al.* showed that Ge pre-amorphization accelerated Ni-silicide reaction, while N pre-implantation slowed it down.[37] Additionally, Ge PAI can promote Ti-silicidation,[20] Ti-germanidation,[38] and Ti-germanosilicidation[19] at lower temperatures. Ion implantation before silicidation can modify surface/interface energies and, thus, the diffusion kinetics and diffusion rates for phase growth. Ge ion implantation is expected to produce a uniform amorphous layer (the PAI process is an out-of-equilibrium uniform process).[18] Then, the presence of amorphous layers with an enhanced amount of defects can result in a Ni uniform reaction at lower temperatures. For silicides, the NiSi growth rate on an amorphous Si region is higher than the one on a crystalline Si region.[18] These characteristics enabled the growth of the NiSi phases at lower annealing temperatures. Variations on the NiSi → $NiSi_2$ transformation were also encountered. A high accumulation of Ge in the NiSi/Si interface delayed the $NiSi_2$ growth rate. As Ni-silicide grows, an amount of Ge atoms is repelled out of the silicide layer and pileup at the silicide/Si interface. The Ge concentration can alter the Ni-silicide growth rate to produce a smooth interface, change the interface energies, and delay the phase transformation.[18] Mao *et al.* also verified Ge accumulation along the TiSiGe/Ge interface, when studying Ti-germanosilicidation by means of TEM coupled with Electron Energy Loss Spectroscopy (EELS) analysis and secondary-ion mass spectrometry (SIMS) depth profiles.[19] Here, Ge PAI enhanced the formation of the mono-stanogermanide phase at lower temperatures either when used alone or when combined with C PAI.

Concerning the use of Si PAI, Guihard *et al.* showed by time-resolved x-ray diffraction that for a given implantation dose (1×10^{14} Si/cm^2) and amorphized thickness, the silicide phase sequence can be importantly impacted. Additionally, the Ni deposited thickness had an impact as well. First of all, a large temperature delay in the formation of the metal-rich phases was noticed. Then, NiSi (obtained from 30 nm Ni deposition) growth temperature underwent an abrupt increase. Meanwhile, for samples with 10 nm of Ni deposition, the delay was less important. Finally, PAI samples had a lower onset temperature for $NiSi_2$ phase transformation. In general, the NiSi phase stability temperature range was shortened and the $NiSi_2$ phase appeared at lower temperatures.[39] Özcan *et al.*[36] also verified a modulation on the phase sequence when Si PAI, either at room or at −100 °C, was used prior to Ni-silicide formation. The interest of performing PAI at low temperatures was to increase the damage to the crystal structure. Their results showed a NiSi formation at lower temperatures, by about 25 °C, compared with the non-amorphized substrate. Yet, they considered the impact of Si PAI on kinetics to be negligible and stated that Si implantation into a Si substrate was not expected to have such a significant impact on the diffusion of Ni or Si. In our case, Si PAI slightly delayed the formation of the Ni(GeSn) phase.

Ozcan *et al.* showed, by *in situ* XRD, that C PAI at room temperature delayed NiSi formation by approximately 15 °C.[36] Luo *et al.* also evidenced a delay on the $NiSi_2$ phase formation.[40] It is then likely that the presence of C in the growing silicide film delayed the diffusion of metal and Si atoms during the silicidation reaction.[36] Verifying a delay on NiSi formation was, however, not possible. Indeed, Luo *et al.* studied phase sequences by means of *ex situ* θ–2θ scans with the first annealing conducted at 425 °C. At these temperatures, NiSi formation was already verified, yet the transformation temperature from the Ni-rich to the Ni-monosilicide phase was impossible to obtain. Concerning germanides and stanogermanides, Liu *et al.* evidenced that C PAI can induce certain NiGe or Ni(GeSn) preferred crystalline orientations during the solid-state reaction.[21,41,42] However, their *ex situ* θ–2θ scans were only acquired at high temperatures. Then, the impact of the phase sequence was difficult to determine. In our case, C PAI delayed the Ni(GeSn) phase formation up to 270 °C.

The various interactions that the different implanted ions and the GeSn substrate can have during the amorphization should be considered. A previous study from Rice had already questioned the impact that different ion implants, with differing masses and atomic sizes, might have on the formation of nickel silicides.[43] Rice evaluated and compared the impact of different implanted species, fluorine (F), argon (Ar), and nitrogen (N) on Ni-silicide formation and property evolution. Variations on (i) the amorphous surface, (ii) the amorphization depth in the Si substrate, and (iii) Ni diffusion rates were observed when the implanted ion changed.[43]

In our case, the PAI parameters of the different ions were adapted to obtain the same amorphous GeSn thickness. It was verified that, indeed, the α-GeSn layer thickness was comparable for different samples (see Fig. 4). The local properties of the amorphized GeSn layer can yet vary depending on the ion size, chemical properties, and concentration.

Dopant concentration can be controlled by the modification of the implantation parameters (dose and energies). Indeed, ion fluences and, consequently, the ion concentration in the layers can have an impact on the structural and morphological evolution of thin films.[44] The implantation parameters varied from one species to the other to have a comparable amorphized thickness. Then, for a comparable thickness, the ion concentration can vary from one system to the other. This variation on concentration can explain the differences observed due to a variation of segregation or distribution of the implanted ions within the intermetallic.

It is well known that the ion mass can affect the amorphization mechanisms.[28] It has also been reported that lighter atoms (C, for instance) generate less damage than heavier ones (Ge, for

example).[36] Then, due to (i) the diversity of amorphization processes used combined to (ii) the hypothesis made for amorphization process simulation, we cannot fully ensure that the amorphization in the implanted layer is exactly the same for all the species. Such variation can result in damage fluctuations and different diffusion behaviors. The enhancement of diffusion is, however, dependent on the size/mass of the implanted species as already mentioned.

The chemical and/or physical interactions occurring between the implanted elements and the intermetallics during the solid-state reaction have also to be considered. Differences on incorporation, distribution, and/or segregation of these elements could modify the phase sequence. Once a crystalline intermetallic is formed [the $Ni_5(GeSn)_3$ rich phase in our case], the mechanism for atom transport might vary. Indeed, the overall mass transport can be impacted by dislocations, grain boundaries (GBs), surface, and interface diffusion of the atoms.[34] Ge implanted atoms were observed to accumulate/segregate at both the NiSi/Si[18] and Ti(SiGe)/Ge interfaces.[19] C, however, is expected to accumulate/segregate at the intermetallic/substrate interfaces and at grain boundaries (GBs).[36,45] The occurence of this segregation/accumulation might modify atom diffusion and thermal stability. Secondary-ion mass spectrometry (SIMS) depth profiles proved that implanted C species were distributed in Ni-silicides,[40] Ni-germanides,[41,42] or Ni-stanogermanides[21] or accumulated at the NiSi/Si,[40] NiGe/Ge,[41,42] and Ni(GeSn)/GeSn interfaces.[21] Moreover, implanted C was observed to segregate at the interfaces of Si/SiGe/Si multi-layered structures. C coming from Co/C/Si and C/Co/Si interlayers[46] and Ni/SiC reactions[47] migrated at GB as well.

The C solubility in Ni, Ge, or Sn is low. The Ni_3C metastable phase can be obtained only at high temperatures (above 1600 °C) and would require the incorporation of around 25 at. % of C to form the phase.[48] For Si–C systems, only the silicon carbide (SiC) compound exists.[48] The amount of C dissolved in Ge has been observed to be low and no evidence of a compound formation was acquired during Ge–C reactions.[49] Meanwhile, Sn can dissolve only traces of carbon which precipitates upon cooling as graphite.[48] Then, the incorporation of implanted C in Ni/GeSn intermetallics should not be favorable and C atoms are expected to be expelled from the lattice. On the other hand, Ge and Si atoms could be, to some extent, incorporated into the Ni-rich or Ni(GeSn) lattice.

There is an important difference in the atomic radii of the different implanted ions. For species used for this study (Si, Ge, and C), the difference in atomic radii (a_r) goes as follows: a_r C = 67 pm $<$ a_r Si = 111 pm $<$ a_r Ge = 125 pm. This parameter might promote a preferential arrangement of the atoms during the phase sequence, as schematically presented in Fig. 5.

The effect of Si PAI on phase nucleation is ambiguous.[36,39] In our case, a slight Ni(GeSn) growth delay was observed when Si PAI was used. The intermediate size of Si compared with Ge and C and its partial solubility in the phases might enable it to homogeneously distribute in different areas of the intermetallic layer at grain boundaries and at the Ni(GeSn)/GeSn interfaces (see Fig. 5). Then, the phase sequence was only slightly impacted.

The larger Ge atomic size and its partial solubility in the phases might prevent it from accumulating at the GB. Implanted Ge will then be incorporated into the phases or will pileup around interfaces (see Fig. 5), modifying the interface states and interface energies, which could be beneficial for the growth of the Ni(GeSn) phase at lower temperatures.

Thanks to their low dimension and their very low solubility, C atoms are expected to preferentially segregate at GB (see Fig. 5). In a previous work,[50] we showed by means of transmission electron microscopy (TEM) images, coupled with energy-dispersive x-ray spectroscopy (EDS) and electron energy loss spectroscopy (EELS) analysis, that Sn segregation occurs around GB. Segregated Sn acted as a diffusion barrier, more precisely as a "stuffed barrier." This phenomenon hampered diffusion, delaying the Ni(GeSn) growth when the Sn content increased. C is, thus, expected to also distribute around GB and act as a diffusion barrier, which might reduce the Ni diffusion rate and hamper the Ni(GeSn) phase formation. The diffusion barrier effect, whatever be the nature of the ion, can be enhanced with the ion concentration. Indeed, a higher concentration of C compared with Ge or Si at GB can further prevent Ni diffusion. In addition to this diffusion impact, carbon, due to its very low solubility, can have an impurity effect, impact the reaction path, and modify the nucleation barrier by modifying the interface and surface energies. A similar behavior was observed with nitrogen in the Ni/Si system.[33]

Combining Ge + C PAI was quite interesting. Compared with C PAI, the temperature for Ni(GeSn) formation was reduced. Compared with Ge PAI, the Ni(GeSn) phase formation was delayed, however. We then expected Ge and C to behave as they will when used alone. C segregation around GB can then reduce atom diffusion for phase formation, while Ge accumulation at the interface might modify the interface energies, helping to nucleate the Ni(GeSn) phase at lower temperatures. The result was then a competition phenomenon that allowed the system to be in an intermediate regime (see Fig. 5).

In summary, in this section, the impact of various ion implantations on the Ni/GeSn solid-state reaction was discussed in terms of species diffusion, impact on substrate, species solubility, and subsequent impact on chemical and physical interactions. It was reported that the phase sequence and the temperature for phase growth were impacted by PAI. These variations, depending on the nature of the implanted ions, can be due to kinetic and/or thermodynamic factors as supported by the analysis of bibliography for silicides and germanides. Section III B will be dedicated to the impact of PAI processes on Sn segregation.

B. Impact on Sn segregation

As highlighted in the Introduction, one of the biggest issues of Ni/GeSn intermetallics is their high metastability. Due to the low solid solubility of Sn in the Ge lattice, i.e., less than 1 at. %, Sn segregation can easily occur if annealing temperatures exceed the Ge–Sn eutectic point (231 °C), the Sn melting point (232 °C), or the GeSn epitaxy temperature. PAI is an out-of-equilibrium thermodynamic process, however. The possibility of Sn atoms having to demix or separate might be low then. However, due to the loss of long-range order, Sn might not remain in the Ge lattice during the phase sequence. Then, it is important to check if PAI resulted in Sn segregation since the occurrence of as-deposited state for the Ni/GeSn samples. It must be underlined that, in this section, the term Sn segregation only refers to long-range diffusion of Sn.

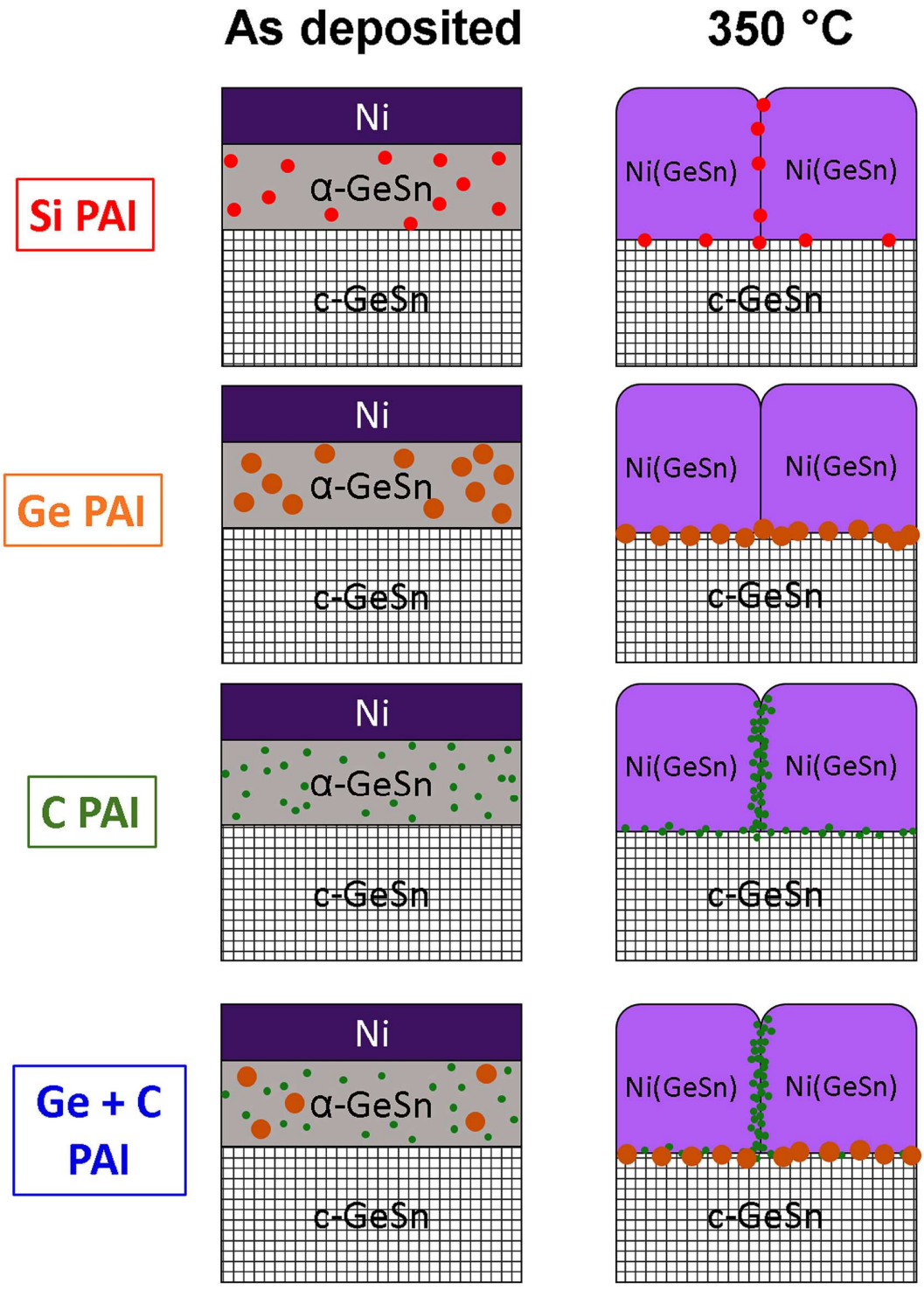

FIG. 5. Schematics representation of Si, Ge, and C ions implanted in a GeSn layer during the phase sequence.

Figure 4 shows the mapping obtained by TEM coupled with EDS for $Ni/Ge_{0.90}Sn_{0.10}$ samples with Ge (top row) and Ge + C (bottom row) PAI in the as-deposited state. TiN, Ni, amorphous α-GeSn, crystalline c-GeSn, and Ge layers were well identified in the as-deposited images for both samples. Sn was observed to be homogeneously distributed in the α-GeSn and c-GeSn layers. The α-GeSn thickness for the Ge PAI samples was 17 ± 1 nm, while for the Ge + C PAI samples, it was 19 ± 1 nm. Additionally, intermixing layers with Ni, Ge, and Sn atoms located between the Ni layer and α-GeSn were present in both samples. No accumulation of Sn was observed at the interfaces and the surface. Thus, PAI prior to metallization did not trigger Sn segregation; at least no Sn diffusion at a long-range scale was evidenced. Ni diffusion happened since the occurrence of the as-deposited state. For Ge PAI, the thickness of the intermixing layer was about 8 ± 1 nm, while for the Ge + C PAI sample, it was about 7 ± 1 nm. A comparable initial state was, thus, confirmed for both samples.

As a complement, XRD analyses were systematically performed on samples in the as-deposited state and annealed, by RTA, from 150 up to 550 °C. The Sn segregation threshold temperature was extracted from the XRD patterns when peaks related to β-Sn were detected. A summary of the obtained results is plotted in Fig. 6.

In the as-deposited state, no Sn segregation was observed by *ex situ* XRD scans on the implanted samples, whatever may be the implanted species. There was no Sn segregation on the reference sample either. Then, implantation at the energies used did not destabilize the metastable GeSn layers in terms of Sn segregation. In this way, XRD analyses comfort the observations made by TEM/EDS (see Fig. 4). For the non-implanted samples, peaks due to β-Sn segregation were observed for annealing at 350 °C and above. Ge implantation did not modify the segregation threshold and peaks due to β-Sn segregation were observed at temperatures of 350 °C and above as well. Si implantation slightly delayed Sn segregation for 50–100 °C. Meanwhile, for samples with C PAI, Sn diffraction lines were not observed up to anneals at 500 °C. C PAI seemed to push up the Sn segregation threshold by 150 to 200 °C, which is remarkable for these kinds of layers. Gaiduk *et al.* showed that C implantation in the Si/SiSn/Si multi-layers resulted in good crystalline quality and almost complete (90–95%) incorporation of the Sn atoms into lattice positions of the Si matrix in which Sn segregation and precipitation was suppressed.[51] The comparison between SiSn and GeSn systems has to be taken with a note of caution, however, as the solubility of Sn is different in Si and Ge.

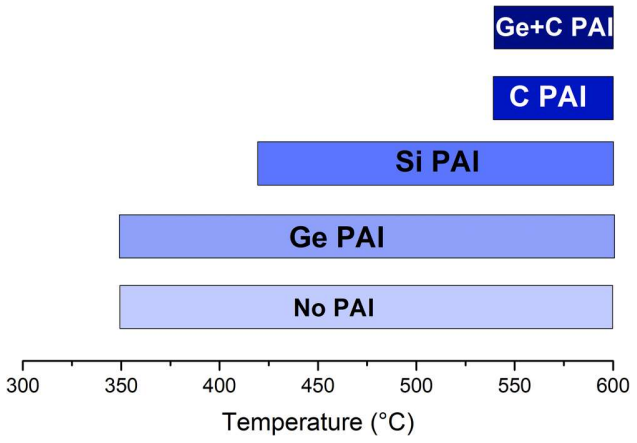

FIG. 6. Sn segregation threshold temperatures extracted from XRD analyses of samples annealed by RTA. N.B.: The values of Sn segregation threshold only refer to long-range diffusion of Sn.

Differences concerning segregation and distribution for the different ions implanted discussed earlier and schematized in Fig. 5 could explain Sn segregation temperature threshold variations. We previously showed that Sn segregation in Ni/GeSn intermetallics occurred in two steps.[50] First, Sn accumulated at grain boundaries (GBs) and near the intermetallic/GeSn interface. Later, when the annealing temperatures were high enough, Sn migrated toward the surface.[50] Ge accumulation at the Ni(GeSn)/GeSn interface would not modify the diffusion paths for Sn segregation. Then, the Sn segregation threshold was not impacted. Meanwhile, C preferential accumulation at grain boundaries could act as a diffusion barrier to Sn motion, slowing down segregation and postponing it to higher temperatures. Finally, a portion of Si atoms might accumulate at GB (see Fig. 5). This distribution is supposed to delay, up to a certain extent, Sn segregation. Globally, the effects on Sn segregation could be related to the size of the implanted species as observed for the phase sequence during the solid-state reaction.

In this section, it was observed that PAI step, prior to Ni metallization, generated an amorphous GeSn layer in which Sn remained homogeneously distributed. Additionally, higher threshold temperatures for Sn segregation were observed in the Si, C, and Ge + C PAI samples. The accumulation of Si or C atoms at GB can delay the threshold temperature for Sn segregation. These species can hamper Sn diffusion and avoid its propagation toward the surface. It is, however, important to underline that, if the obtained results did not enable to evidence Sn segregation caused by Sn diffusion (long scale phenomenon), the possibility of local segregation cannot be totally discarded. The use of more local characterization techniques such as Atom Probe Tomography (APT) might be very useful for observing potential Sn clustering or precipitates.

C. Impact on surface morphology

Figure 7 shows AFM images obtained for all types of samples annealed at various temperatures by RTA. Whatever be the system studied, at low temperature (i.e., for $T \leq 300$ °C), samples exhibited a cross-hatch pattern along the $\langle 110 \rangle$ crystallographic directions. This pattern resulted from the propagation of the 60° threading arms of misfit dislocations on (1 1 1) planes.[22,52] Thus, this surface morphology directly originates from the epitaxy of GeSn layers on the Ge virtual substrates underneath. In the as-deposited state, the Ni and TiN layers were extremely smooth and their deposition did not modify the original surface morphology. On the other hand, whatever be the PAI treatment, the cross-hatch pattern was not affected. The implantation doses were, thus, sufficiently low to prevent surface degradation. Such behavior was also observed by Gaiduk *et al.* when investigating the impact of C implantation on

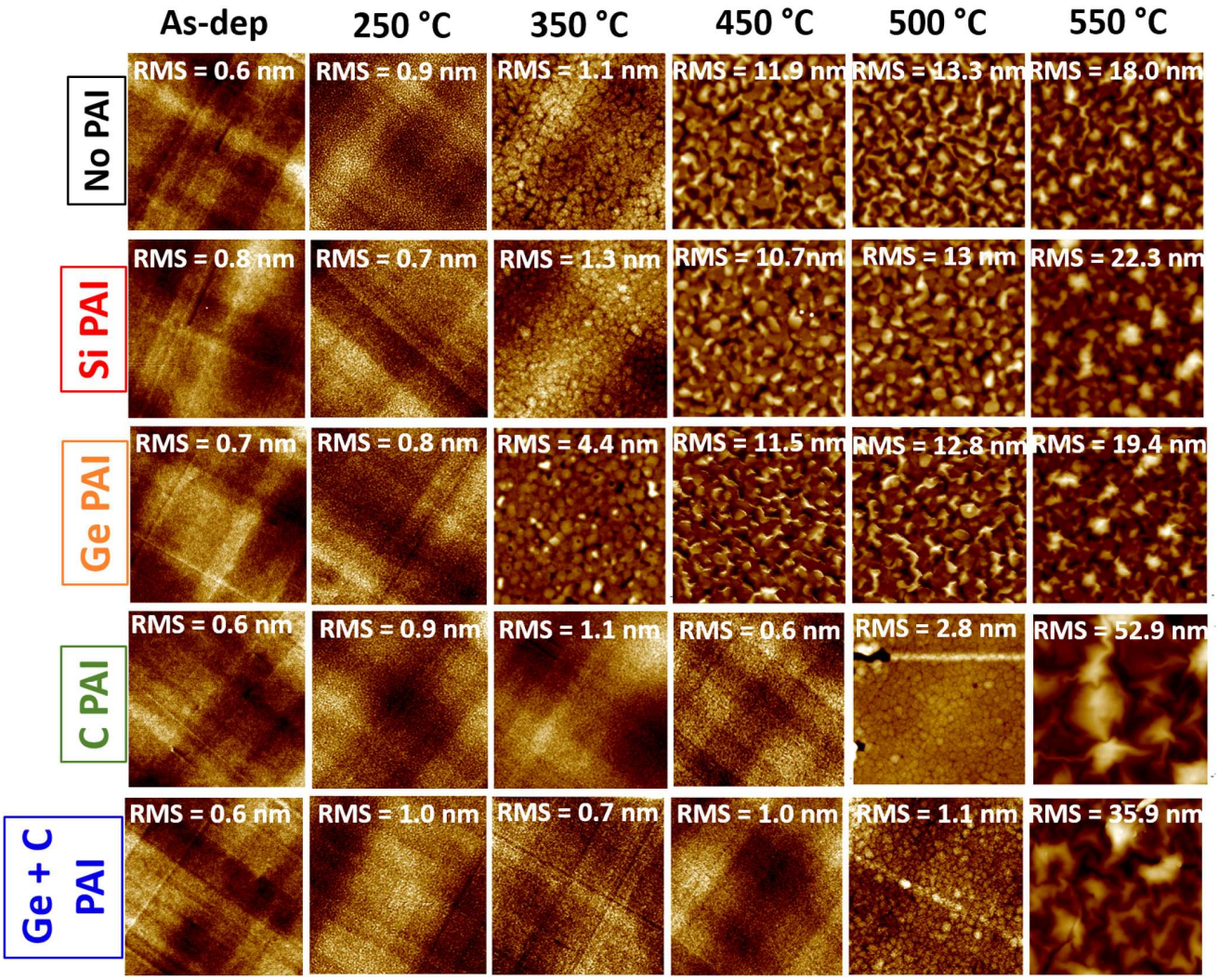

FIG. 7. AFM images (scan size $5 \times 5\,\mu m^2$) of the surface of samples annealed at various temperatures for the Ni/GeSn systems without PAI and with different PAI treatments.

the stability of the Si/SiSn/Si layers, in which the crystalline quality was preserved after implantation.[51]

The cross-hatch morphology was preserved up to 300 °C, meaning that the formation of the Ni-rich phase did not modify the original morphology. At 350 °C, the surface morphology for the $Ni/Ge_{0.9}Sn_{0.1}$ reference system changed. Micro-cracks at the sub-micrometer scale were observed together with an increase of the surface RMS (root mean squared) roughness values as seen in Fig. 7. This change was linked to the formation of the monostanogermanide phase, the start of grain-boundary grooving, and the subsequent agglomeration.

At higher temperatures, the roughness values gradually increased due to two phenomena: further agglomeration and Sn segregation. The surface morphological evolution observed for samples with Si and Ge PAI was very similar and comparable to the reference sample. Thus, the implantation of these species did not significantly modify the morphological evolution with temperature compared with the reference.

The Sn segregation threshold temperature was modified when Si PAI was used, however. The morphological evolution was, therefore, mainly due to the agglomeration of the Ni(GeSn) phase. Sn segregation increased the morphological degradation. In contrast, Tsui *et al.* were able to effectively suppress NiSi agglomeration and maintain smooth interfaces when Ge PAI was used.[18] One important aspect to consider is the difference in the degradation mechanisms between silicides and germanides/stanogermanides. For

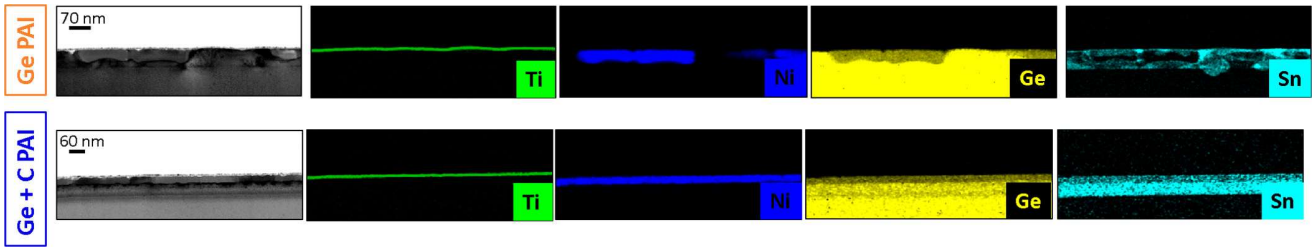

FIG. 8. Cross-sectional TEM images, coupled with an EDS analysis of Ni/GeSn samples with Ge PAI (top row) and Ge + C PAI (bottom row), annealed at 350 °C.

silicides, degradation occurs because of two phenomena (i) agglomeration of the NiSi layer and (ii) nucleation of the $NiSi_2$ phase. An accumulation of Ge in the NiSi/Si interfaces could (i) modify diffusion kinetics and interface energies, (ii) prevent atom diffusion, and (iii) modify the Ni-silicide growth rate to produce a smooth interface, which might delay the $NiSi_2$ formation.[18] As a consequence, the Ni-silicide thermal stability was enhanced.

For germanides/stanogermanides, the growth of such a $NiGe_2$ or $Ni(GeSn)_2$ is not expected to occur due to thermodynamic impediments. Degradation of these kinds of films starts due to grain boundary grooving up to the agglomeration process. Then, Ge incorporated into the intermetallic phases and/or accumulated at the Ni(GeSn)/GeSn interface is not expected to influence the agglomeration process.

Great differences were highlighted in samples with C implantation. The cross-hatch pattern was still visible up to 450 °C annealing together with low RMS roughness values. At 500 °C, the grain-boundary grooving started. Finally, at 550 °C, layers agglomerated. A similar morphological stability improvement was evidenced for C implantation in Si,[36] Ge,[41,42] or GeSn.[21] Here, C preferential segregation at grain boundaries (due to its very low solubility in intermetallic phases) might reduce the grain-boundary grooving rates and delay the agglomeration of the layers. Indeed, C in GB is likely to influence grain-boundary energy and grain-boundary diffusion. One can expect that C will enhance the grain-boundary cohesion and, thus, lower the grain-boundary energy, delaying the agglomeration process.[46]

In order to complement the AFM results, TEM–EDS analyses were performed on samples with Ge and Ge + C PAI and annealed at 350 °C for 30 s in a N_2 environment. The results are shown in Fig. 8.

For the Ge PAI sample, the Ni(GeSn) layer lost its continuity due to agglomeration at this temperature. The grains were mainly made of Ni and Ge atoms. Meanwhile, Sn started to accumulate around the grains and near the surface. An agglomeration of the GeSn layer underneath was also observed and Sn also started to segregate. Meanwhile, for the Ge + C PAI sample, a very different scenario took place. A continuous 29 ± 1 nm thick Ni(GeSn) polycrystalline layer was observed in which no agglomeration or Sn segregation happened. C implantation was, thus, demonstrated to positively impact the surface morphology evolution by delaying agglomeration and Sn segregation. In addition, the GeSn layer stayed intact.

The reduction of the grain size of intermetallic phases can reduce the agglomeration processes.[53,54] Indeed, models that explain agglomeration mechanisms in thin films stated that the grain-boundary grooving was linked to grain size and that a reduction of the grain size might reduce agglomeration.[53,54] On the other hand, the average grain size is smaller for silicides formed on α-Si than that on single-crystal Si in samples subjected to the same heat treatments.[55] Additionally, a reduction in crystallite size, when PAI was performed, was observed by different groups. Chen *et al.* observed this phenomenon when studying the effects of PAI on Ni-silicide formation,[56] Duan *et al.* did so when using fluorine (F) PAI on Ge for NiGe formation,[57] and Mao *et al.* when analyzing NiPt-germanosilicidation with Ge PAI.[55] The full width at half maximum (FWHM) of the Ni-mono-stanogermanide was, therefore, measured from various XRD patterns obtained during *in situ* measurements of the different systems. The results are provided in Fig. 9.

Two families of data are obvious: FWHM values for the Ni (GeSn) phase, with a C PAI step, were higher than the ones for the

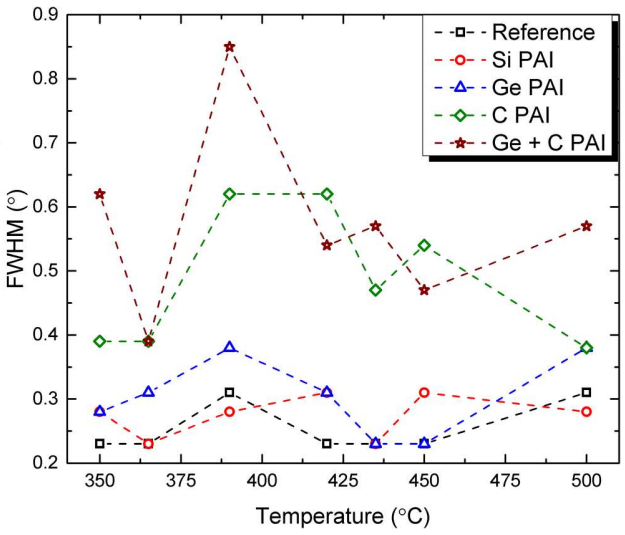

FIG. 9. Evolution of the FWHM values collected for the Ni mono-stanogermanide peak around 53.5 ° from various *in situ* XRD measurements for Ni/GeSn systems without and with various PAI treatments.

reference, Si PAI, and Ge PAI systems. According to the Scherrer equation, the crystallite size is inversely proportional to the FWHM.[58] This means that the grain size of the mono-stanogermanide was reduced due to C ion implantation into the layer, which was clearly beneficial for delaying agglomeration and enhancing the morphological stability of the layers. Our results, obtained using θ–2θ XRD scans, enabled the discussion the grain size in terms of thickness. The lateral size was not considered since it implies in-plane measurements. Such a characterization might be useful for discussing the impact of C impurities not only in terms of GB diffusion paths but also in terms of GB volume.

In summary, in this section, it was shown that the use of Si or Ge implantation did not significantly impact the surface morphology of the layers. In particular, these species had a limited effect on the Ni(GeSn) agglomeration process. On the other hand, the implantation of C positively impacted the surface morphology evolution by delaying Sn segregation and Ni(GeSn) agglomeration. Due to its very low solubility in the intermetallic phases, C atoms were mainly confined in the grain boundaries and had a strong impact on the GB diffusion paths.

D. Impact on the electrical properties

The evolution of the sheet resistance (R_{sh}) after various RTA techniques from 150 up to 550 °C was investigated. This should help us to understand the impact of phase sequence variations and morphological evolutions on electrical properties. The results for all systems are presented in Fig. 10.

Whatever be the system observed, from the as-deposited state and up to 200 °C, the R_{sh} values remained constant at around 28–35 Ω/sq. At 250 °C, a slight R_{sh} increase was observed. This increase was linked to the Ni-rich phase growth. After this, resistivities decreased due to the growth of the Ni(GeSn) phase (a less resistive phase of the Ni/GeSn system). At 350 °C, minimum values were reached for all samples. Beyond 350 °C, a strong increase of the R_{sh} values occurred for samples without PAI and with Ge or Si PAI. This behavior can be directly linked to the degradation of the Ni(GeSn) layers, observed in Fig. 7, and due to agglomeration. Later on, Sn segregation further degraded the electrical properties. Thus, as observed for the morphological thermal stability, the Si or Ge PAI process did not significantly impact the electrical properties' evolution with the annealing temperature.

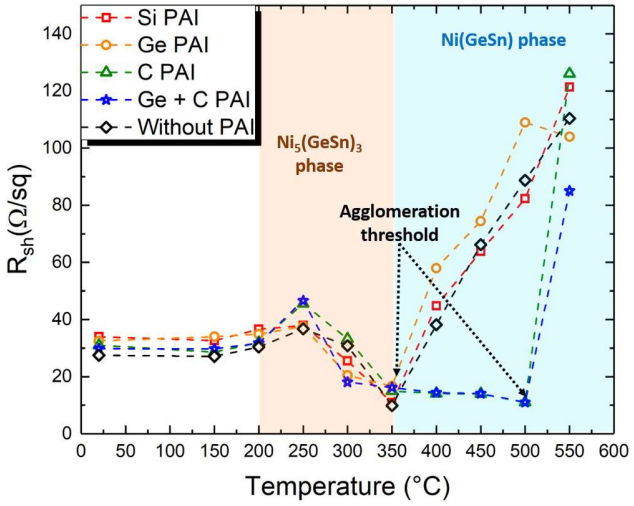

FIG. 10. Evolution of the sheet resistance as a function of the rapid thermal annealing temperature for Ni/GeSn without and with various PAI treatments.

Si PAI on Si substrates degraded NiSi electrical properties. R_{sh} values increased more at lower temperatures than that for reference samples.[36] On the other hand, Ge PAI yielded, generally, lower R_{sh} for Ti-germanides and Ti-germanosilicides.[19,38] Meanwhile, Ge PAI on Si substrates improved NiSi electrical thermal stability.[18] Indeed, Tsui *et al.* evidenced a delay on NiSi agglomeration and $NiSi_2$ formation. Indeed, Tsui *et al.* evidenced a delay on NiSi agglomeration and NiSi2 formation that were main reasons for NiSi contact degradation. As evidenced earlier, Ge or Si PAI is not expected to modify grain boundary grooving and the agglomeration process during Ni-stanogermanidation. Then, the degradation of the electrical properties can occur similar to that for the reference samples.

On the other hand, an increase of the electrical thermal stability was evidenced with C PAI in different systems such as Ni-silicides,[36,45] Ni-germanides,[41,42] and Ni-stanogermanides.[21] Ni/GeSn samples with C PAI had a larger process window over which the R_{sh} values remained low and stable. Indeed, a plateau was observed from 300 up to 500 °C for the Ge + C PAI sample and from 350 up to 500 °C for the C PAI sample. The earlier reduction of R_{sh} values for the Ge + C PAI system can be related to the Ni(GeSn) phase growth at lower temperatures. Beyond 500 °C, the sheet resistance drastically increased because of agglomeration and Sn segregation.

It was, thus, evidenced that the deterioration of electrical properties was linked to Ni(GeSn) layer agglomeration, with Sn segregation worsening than degradation. On the other hand, C implantation had the ability to delay agglomeration and Sn segregation, thanks to the preferential segregation/accumulation at grain boundaries. This phenomenon was then highly beneficial for preserving electrical stability.

IV. CONCLUSIONS

In this work, the impact of Si, Ge, and C PAI on the Ni/GeSn phase sequence, Sn segregation, and morphological and electrical properties during the solid-state reaction was analyzed. As far as the phase sequence was concerned, the overall evolution was comparable. The $Ni_5(GeSn)_3$ phase was obtained first, followed by the mono-stanogermanide phase Ni(GeSn), for all the systems.

The impact of PAI on the Ni/GeSn solid-state reaction was discussed in terms of species diffusion, impact on substrate, species solubility, and subsequent impact on chemical and physical interactions. Phase sequence and temperature for phase growth were impacted by PAI. It was discussed that these variations, depending on the nature of the implanted ions, could be related to kinetic and/or thermodynamic factors, as supported by the analysis of bibliography for silicides and germanides.

The use of Si or Ge implantation had no significant impact on the surface morphology of the layers. In particular, these species had a limited impact on the Ni(GeSn) agglomeration process. On the other hand, the implantation of C positively impacted the surface morphology evolution by delaying Sn segregation and Ni (GeSn) agglomeration. Due to its very low solubility in the intermetallic phases, C was mainly confined to grain boundaries, with a strong impact on the GB diffusion paths.

Finally, the deterioration of electrical properties as the RTA temperature increased was linked to layer agglomeration, with Sn segregation worsening than degradation. C implantation had the ability to delay agglomeration and Sn segregation, thanks to preferential segregation/accumulation at the grain boundaries. This phenomenon was highly beneficial for preserving electrical stability in an enhanced process window.

The combination of Ge and C PAI prior to GeSn metallization is, thus, an interesting option for obtaining the less resistive phase, Ni(GeSn), at low temperatures and with enhanced thermal stability. This could also act as a solution benefiting from high quality and stable GeSn-based metallic contacts that are CMOS-compatible and could be integrated in electronic or opto-electronic components.

ACKNOWLEDGMENTS

The authors would like to thank N. Chevalier and D. Mariolle (CEA Leti) for their support during the AFM measurements and M. Coig (CEA Leti) for her assistance during ion implantation. This work was supported by the French National Research Agency (ANR) under the "Investissements d'avenir" programs: Nos. ANR 10-AIRT-0005 (IRT NANOELEC) and ANR 10-EQPX-0030 (EQUIPEX FDSOI 11).

DATA AVAILABILITY

The data that support the findings of this study are available from the corresponding author upon reasonable request.

REFERENCES

[1]S. Wirths, D. Buca, and S. Mantl, "Si-Ge-Sn alloys: From growth to applications," Prog. Cryst. Growth Charact. Mater. **62**(1), 1–39 (2016).
[2]S. Zaima, O. Nakatsuka, N. Taoka, M. Kurosawa, W. Takeuchi, and M. Sakashita, "Growth and applications of GeSn-related group-IV semiconductor materials," Sci. Technol. Adv. Mater. **16**(4), 043502 (2015).
[3]S. Wirths, R. Troitsch, G. Mussler, J.-M. Hartmann, P. Zaumseil, T. Schroeder, S. Mantl, and D. Buca, "Ternary and quaternary Ni(Si)Ge(Sn) contact formation for highly strained Ge p- and n-MOSFETs," Semicond. Sci. Technol. **30**(5), 055003 (2015).
[4]S. Wirths, R. Geiger, N. von den Driesch, G. Mussle, T. Stoica, S. Mantl, Z. Ikonic, M. Luysberg, S. Chiussi, J. M. Hartmann, H. Sigg, J. Faist, D. Buca, and D. Grützmacher, "Lasing in direct-bandgap GeSn alloy grown on Si," Nat. Photonics **9**(2), 88–92 (2015).
[5]J. Demeulemeester, A. Schrauwen, O. Nakatsuka, S. Zaima, M. Adachi, Y. Shimura, C. M. Comrie, C. Fleischmann, C. Detavernier, K. Temst, and A. Vantomme, "Sn diffusion during Ni germanide growth on $Ge_{1-x}Sn_x$," Appl. Phys. Lett. **99**(21), 211905 (2011).
[6]S. Wirths, R. Troitsch, G. Mussler, P. Zaumseil, J.-M. Hartmann, T. Schroeder, S. Mantl, and D. Buca, "Ni(SiGeSn) metal contact formation on low bandgap strained (Si)Ge(Sn) semiconductors," ECS Trans. **64**(6), 107–112 (2014).
[7]J. Zheng, Y. Zhang, Z. Liu, Y. Zuo, C. Li, C. Xue, B. Cheng, and Q. Wang, "Fabrication of low-resistance Ni ohmic contacts on n^+-$Ge_{1-x}Sn_x$," IEEE Trans. Electron Devices **65**(11), 4971–4974 (2018).
[8]L. Wang, G. Han, S. Su, Q. Zhou, Y. Yang, P. Guo, W. Wang, Y. Tong, P. Shi Ya Lim, B. Liu, E. Yu-Jing Kong, C. Xue, Q. Wang, B. Cheng, and Y.-C. Yeo, "Thermally stable multi-phase nickel-platinum stanogermanide contacts for germanium-tin channel MOSFETs," Electrochem. Solid State Lett. **15**(6), H179–H181 (2012).
[9]M. Noroozi, M. Moeen, A. Abedin, M. S. Toprak, and H. H. Radamson, "Effect of strain on Ni-$(GeSn)_x$ contact formation to GeSn nanowires," MRS Proc. **1707**, 7–12 (2014).
[10]A. Quintero, P. Gergaud, J. Aubin, J.-M. Hartmann, V. Reboud, and P. Rodriguez, "Ni/GeSn solid-state reaction monitored by combined x-ray diffraction analyses: Focus on the Ni-rich phase," J. Appl. Cryst. **51**(4), 1133–1140 (2018).
[11]D. Mangelinck, J. Y. Dai, J. S. Pan, and S. K. Lahiri, "Enhancement of thermal stability of NiSi films on (100)Si and (111)Si by Pt addition," Appl. Phys. Lett. **75**(12), 1736–1738 (1999).
[12]F. A. Geenen, K. van Stiphout, A. Nanakoudis, S. Bals, A. Vantomme, J. Jordan-Sweet, C. Lavoie, and C. Detavernier, "Controlling the formation and stability of ultra-thin nickel silicides—An alloying strategy for preventing agglomeration," J. Appl. Phys. **123**(7), 075303 (2018).
[13]C.-H. Cheng and C.-L. Hsin, "A novel silicide and germanosilicide by NiCo alloy for Si and SiGe source/drain contact with improved thermal stability," CrystEngComm **16**, 10933–10936 (2014).
[14]P. Rodriguez, F. Deprat, C. Sésé, S. Zhiou, S. Favier, C. Fenouillet-Béranger, T. Luo, D. Mangelinck, P. Gergaud, and F. Nemouchi, "Phase formation sequence and cobalt behavior in the $Ni_{0.9}Co_{0.1}$ system during the thin film solid-state formation," Microelectron. Eng. **200**, 19–25 (2018).
[15]A. Quintero, P. Gergaud, J. Aubin, J.-M. Hartmann, N. Chevalier, J.-P. Barnes, V. Loup, V. Reboud, F. Nemouchi, and P. Rodriguez, "Impact of Pt on the phase formation sequence, morphology and electrical properties of Ni(Pt)/$Ge_{0.9}Sn_{0.1}$ system during solid-state reaction," J. Appl. Phys. **124**(8), 085305 (2018).
[16]A. Quintero, P. Gergaud, J.-M. Hartmann, V. Reboud, E. Cassan, and P. Rodriguez, "Impact of alloying elements (Co, Pt) on nickel stanogermanide formation," Mater. Sci. Semicond. Process. **108**, 104890 (2020).
[17]L. Lachal, P. Rodriguez, M. Grégoire, E. Ghegin, F. Milesi, M. Coig, J. Borrel, S. Joblot, M. Juhel, F. Nemouchi, and F. Mazen, "Effects of pre-amorphization thickness and carbon implantation on NiPt/Si silicidation process," in *22nd International Conference on Ion Implantation Technology (IIT-2018)* (IEEE, 2018), pp. 54–57.
[18]B.-Y. Tsui, C.-M. Hsieh, Y.-R. Hung, Y. Yang, R. Shen, S. Cheng, and T. Lin, "Improvement of the thermal stability of NiSi by germanium ion implantation," J. Electrochem. Soc. **157**(2), H137–H143 (2010).
[19]S. Mao, G. Wang, J. Xu, D. Zhang, X. Luo, W. Wang, D. Chen, J. Li, A. Du, C. Zhao, T. Ye, and J. Luo, "Improved Ti germanosilicidation by Ge preamorphization implantation (PAI) for advanced contact technologies," Microelectron. Eng. **201**, 1–5 (2018).
[20]S. Mao, G. Wang, J. Xu, X. Luo, D. Zhang, N. Duan, S. Liu, W. Wang, D. Chen, J. Li, C. Zhao, T. Ye, and J. Luo, "Impact of Ge preamorphization implantation on both the formation of ultrathin $TiSi_x$ and the specific contact resistivity in $TiSi_x$/n-Si contacts," IEEE Trans. Elect. Dev. **65**(10), 4490–4498 (2018).
[21]Q. Liu, W. Geilei, Y. Guo, X. Ke, H. Radamson, H. Liu, C. Zhao, and J. Luo, "Improvement of the thermal stability of nickel stanogermanide by carbon prestanogermanidation implant into GeSn substrate," ECS J. Solid State Sci. Technol. **4**(3), P67–P70 (2015).
[22]J. Aubin, J. M. Hartmann, J. P. Barnes, J. B. Pin, and M. Bauer, "Very low temperature epitaxy of heavily *in situ* phosphorous doped Ge layers and high Sn content GeSn layers," ECS J. Solid State Sci. Technol. **6**(1), P21–P26 (2017).
[23]M. Posselt and J. P. Biersack, "Computer simulation of ion implantation into crystalline targets," Nucl. Instrum. Methods Phys. Res. B **64**, 706–710 (1992).

[24]S. Koffel, "Implantation, diffusion et activation des dopants dans le germanium," Ph.D. thesis (Grenoble INPG, 2008).
[25]P. E. Raynal, A. Quintero, V. Loup, P. Rodriguez, L. Vallier, J. Aubin, J.-M. Hartmann, N. Chevalier, and P. Besson, "GeSn surface preparation by wet cleaning and *in situ* plasma treatments prior to metallization," Microelectron. Eng. **203–204**, 38–43 (2019).
[26]A. Nash and P. Nash, "The Ge-Ni (germanium-nickel) system," Bull. Alloy Phase Diagrams **8**(3), 255–264 (1987).
[27]*Defects in Materials and Devices*, edited by D. M. Fleetwood, S. T. Pantelides, and R. D. Schrimpf (CRC Press, 2009).
[28]L. Pelaz, L. A. Marqués, and J. Barbolla, "Ion-beam-induced amorphization and recrystallization in silicon," J. Appl. Phys. **96**(11), 5947–5976 (2004).
[29]S. Gaudet, C. Coia, P. Desjardins, and C. Lavoie, "Metastable phase formation during the reaction of Ni films with Si(001): The role of texture inheritance," J. Appl. Phys. **107**(9), 093515 (2010).
[30]S. Gaudet, P. Desjardins, and C. Lavoie, "The thermally-induced reaction of thin Ni films with Si: Effect of the substrate orientation," J. Appl. Phys. **110**(11), 113524 (2011).
[31]F. A. Geenen, E. Solano, J. Jordan-Sweet, C. Lavoie, C. Mocuta, and C. Detavernier, "The influence of alloying on the phase formation sequence of ultra-thin nickel silicide films and on the inheritance of texture," J. Appl. Phys. **123**(18), 185302 (2018).
[32]K. van Stiphout, F. A. Geenen, N. M. Santos, S. M. C. Miranda, V. Joly, J. Demeulemeester, C. Detavernier, F. Kremer, L. M. C. Pereira, K. Temst, and A. Vantomme, "Impurity-enhanced solid-state amorphization: The Ni-Si thin film reaction altered by nitrogen," J. Phys. D: Appl. Phys. **52**, 145301 (2019).
[33]K. van Stiphout, F. A. Geenen, N. M. Santos, S. M. C Miranda, V. Joly, J. Demeulemeester, C. Mocuta, C. M. Comrie, C. Detavernier, L. M. C Pereira, K. Temst, and A. Vantomme, "Ion beam modification of the Ni-Si solid-phase reaction: The influence of substrate damage and nitrogen impurities introduced by ion implantation," J. Phys. D: Appl. Phys. **54**(1), 015307 (2021).
[34]P. Gas and F. D'Heurle, "Diffusion in silicides: Basic approach and practical applications," in *Silicides: Fundamentals and Applications*, edited by L. Miglio (World Scientific Publishing, 2000), pp. 34–51.
[35]S. W. Jones, *Diffusion in Silicon* (IC Knowledge LLC, 2008).
[36]A. S. Özcan, D. Wall, J. Jordan-Sweet, and C. Lavoie, "Effects of temperature dependent pre-amorphization implantation on NiPt silicide formation and thermal stability on Si(100)," Appl. Phys. Lett. **102**(17), 172107 (2013).
[37]J. A. Kittl, A. Lauwers, O. Chamirian, M. Van Dal, A. Akheyar, M. De Potter, R. Lindsay, and K. Maex, "Ni- and Co-based silicides for advanced CMOS applications," Microelectron. Eng. **70**(2–4), 158–165 (2003).
[38]X. Luo, G. Wang, J. Xu, N. Duan, S. Mao, S. Liu, J. Li, W. Wang, D. Chen, C. Zhao, T. Ye, and J. Luo, "Impact of Ge pre-amorphization implantation on forming ultrathin $TiGe_x$ on both n- and p-Ge substrate," Jpn. J. Appl. Phys. **57**, 07MA02 (2018).
[39]M. Guihard, P. Turcotte-Tremblay, S. Gaudet, C. Coïa, S. Roorda, P. Desjardins, C. Lavoie, and F. Schiettekatte, "Controlling nickel silicide phase formation by Si implantation damage," Nucl. Instrum. Methods Phys. Res. B **267**(8), 1285–1289 (2009).
[40]J. Luo, Z.-J. Qiu, J. Deng, C. Zhao, J. Li, W. Wang, D. Chen, D. Wu, M. Östling, T. Ye, and S.-L. Zhang, "Effects of carbon pre-silicidation implant into Si substrate on NiSi," Microelectron. Eng. **120**, 178–181 (2014).
[41]Q. Liu, G. Wang, Y. Guo, X. Ke, H. Radamson, H. Liu, C. Zhao, and J. Luo, "Effects of carbon pre-germanidation implant into Ge on the thermal stability of NiGe films," Microelectron. Eng. **133**, 6–10 (2015).
[42]Q. Liu, G. Wang, N. Duan, H. Radamson, H. Liu, C. Zhao, and J. Luo, "Effects of carbon pre-germanidation implantation on the thermal stability of NiGe and dopant segregation on both n- and p-type Ge substrate," ECS J. Solid State Sci. Technol. **4**(5), P119–P123 (2015).
[43]J. H. Rice, "The effect of the dose and energy of a pre-silicide implant on nickel silicide formation," AIP Conf. Proc. **1066**, 517 (2008).
[44]R. Choudhary and R. P. Chauhan, "Nitrogen ion implantation effects on the structural, optical and electrical properties of CdSe thin film," J. Mater. Sci. Mater. Electron. **29**, 12595–12602 (2018).
[45]O. Nakatsuka, K. Okubo, A. Sakai, M. Ogawa, Y. Yasuda, and S. Zaima, "Improvement in NiSi/Si contact properties with C-implantation," Microelectron. Eng. **82**(3), 479–484 (2005).
[46]C. Detavernier, R. L. Van Meirhaeghe, H. Bender, O. Richard, B. Brijs, and K. Maex, "$CoSi_2$ formation in the presence of carbon," J. Appl. Phys. **92**, 1207 (2002).
[47]K. De Keyser, B. De Schutter, C. Detavernier, V. Machkaoutsan, M. Bauer, J. Jordan Sweet, S. G. Thomas, and C. Lavoie, "Phase formation and texture of nickel silicides on $Si_{1-x}C_x$ epilayers," Microelectron. Eng. **88**, 536–540 (2011).
[48]M. Hansen and K. Anderko, *Constitution of Binary Alloys* (McGraw-Hill Book Company, 1958).
[49]R. I. Scace and G. A. Slack, "Solubility of carbon in silicon and germanium," J. Chem. Phys. **30**(6), 1551–1555 (1959).
[50]A. Quintero, P. Gergaud, J.-M. Hartmann, V. Delaye, V. Reboud, E. Cassan, and P. Rodriguez, "Impact and behavior of Sn during the Ni/GeSn solid-state reaction," J. Appl. Cryst. **53**(3), 605–613 (2020).
[51]P. I. Gaiduk, J. Lundsgaard Hansen, A. Nylandsted Larsen, F. L. Bregolin, and W. Skorupa, "Suppression of tin precipitation in SiSn alloy layers by implanted carbon," Appl. Phys. Lett. **104**, 231903 (2014).
[52]J. Aubin and J. M. Hartmann, "GeSn growth kinetics in reduced pressure chemical vapor deposition from Ge_2H_6 and $SnCl_4$," J. Cryst. Growth **482**, 30–35 (2018).
[53]D. J. Srolovitz and S. A. Safran, "Capillary instabilities in thin films. I. Energetics," J. Appl. Phys. **60**(1), 247–254 (1986).
[54]K. T. Miller, F. F. Lange, and D. B. Marshall, "The instability of polycrystalline thin films: Experiment and theory," J. Mater. Res. **5**(1), 151–160 (1990).
[55]S. Mao, C. Zhao, G. Wang, J. Xu, X. Luo, D. Zhang, W. Wang, D. Chen, J. Li, T. Ye, and J. Luo, "Impacts of Ge preamorphization implantation and Si capping on the specific contact resistivity of Ni(Pt)SiGe/p^+-SiGe contacts," IEEE Trans. Electron Devices **66**(10), 4331–4336 (2019).
[56]P. H. Chen, C. C. Hsu, J. Lai, B. Liao, C. L. Lin, O. Huang, C. C. Chiu, C. M. Hsu, and J. Y. Wu, "Investigation pre-amorphization implantation on nickel silicide formation," in *IEEE International Interconnect Technology Conference (IITC-2014)* (IEEE, 2014), pp. 249–252.
[57]N. Duan, G. Wang, J. Xu, S. Mao, X. Luo, D. Zhang, W. Wang, D. Chen, J. Li, S. Liu, C. Zhao, T. Ye, and J. Luo, "Enhancing the thermal stability of NiGe by prior-germanidation fluorine implantation into Ge substrate," Jpn. J. Appl. Phys. **57**(5), 07MA03 (2018).
[58]B. D. Cullity, *Elements of X-ray Diffraction* (Addison Wesley Publishing Company, 1956).